Chinese Chemical Letters 34 (2023) 107767

Contents lists available at ScienceDirect

Chinese Chemical Letters

journal homepage: www.elsevier.com/locate/cclet

Amorphous hollow carbon film as a flexible host for liquid Na-K alloy anode

Meng Shao[1], Ningxiang Wu[1], Tianming Chen, Xu Han, Yu Shen, Weina Zhang, Bing Zheng, Sheng Li*, Fengwei Huo*

Key Laboratory of Flexible Electronics (KLOFE) and Institute of Advanced Materials (IAM), Nanjing Tech University (NanjingTech), Nanjing 211800, China

ARTICLE INFO

Article history:
Received 10 May 2022
Revised 25 July 2022
Accepted 20 August 2022
Available online 28 August 2022

Keywords:
Carbon defects
Flexible carbon film
Na-K alloy
Hollow carbon spheres
K-S battery

ABSTRACT

Compared with solid alkali metal anodes (Li, Na, K), liquid metal anodes (LMAs) could enable high-energy batteries due to their unique advantages, such as self-healing property and no dendrites. Among LMAs, liquid Na-K alloy anode has become a hotspot due to its high theoretical capacity, low redox potential and formation at room temperature (RT). However, it is challenging to utilize liquid Na-K alloy directly and independently as an electrode; and the high surface tension makes it more difficult to immerse into porous current collectors at RT. Herein, an amorphous hollow carbon film (AHCF) consisting of hollow spheres with significant surface defects has been designed to quickly infiltrate Na-K liquid alloy into the hollow carbon film at RT, forming a composite electrode (Na-K@AHCF). The symmetric cell with Na-K@AHCF could exhibit a cycle lifespan up to 400 h at 0.1 mA/cm^2 and achieve stable stripping/deposition even at 5 mA/cm^2. When matching with cathode material of sulfurized polyacrylonitrile (SPAN), the obtained K-S full cell exhibits good cycle stability and rate performance.

© 2023 Published by Elsevier B.V. on behalf of Chinese Chemical Society and Institute of Materia Medica, Chinese Academy of Medical Sciences.

Green energy storage devices have been extensively developed nowadays [1,2]. Specifically, alkali metal (Li, Na, K) batteries have become a research hotspot due to their high theoretical capacities (3861, 1166 and 685 mAh/g) and low redox potentials (−3.04, −2.71 and −2.93 V *vs.* standard hydrogen electrode (SHE)), which can meet the growing demand for high energy density in rechargeable energy storage devices [3–6]. However, dendrite growth and interfacial issues have hindered the practical application of solid-state alkali metal anodes in rechargeable batteries [7–10]. Dendrites may induce safety concerns of short circuits as separator piercing, and the formation of dead metal would bring irreversible capacity fading. In addition, interfacial issues may cause thermal runaway, poor cycle stability and low coulombic efficiency due to the continuous formation of unstable solid electrolyte interfaces (SEI) [11–14].

Various strategies have been devised to address these problems. One of them is the electrolyte modification for SEI stabilization, which mainly studied the concentration and additives of electrolytes [15–18]; another route is the artificial interface construction by designing SEI from atomic/molecular layer deposition or chemical reactions [19,20]. In addition, the application of solid-state electrolytes is also an effective approach [21–25]. Another widely used strategy is preparing nanostructured anode hosts, which aim to build carbon-based or porous metal current collectors [26–28] or metalphilic interlayers [29,30]. However, there are still challenges and large room for improvement of these anodes due to the complex composition of SEI, the interface issues of solid-state electrolytes and the complication of combining the metal anodes and the nanostructure hosts.

Compared with solid metal anodes hindered by the issues mentioned above, liquid metal anode (LMA) is a promising alternative since it is fluidly, dendrite-free, self-healable, and has fast ion transport with high energy density [25,31–38]. Currently, among LMAs, a commercialized application is high-temperature sodium-sulfur (Na-S) batteries, which could be operated at above 300 °C. However, the high operating temperature and expensive thermal management system limit its application range [39], and studying LMAs at room temperature (RT) is necessary.

When the sodium metal content is between 9.2 wt% and 58.2 wt%, the sodium-potassium (Na-K) alloy remains liquid at RT, making it a research hotspot in recent years [40–46]. However, it is hard to serve as an electrode alone due to the high surface tension, fluidity, infinite interface formation and volume change. Thus, the study of Na-K LMA mainly focuses on immobilizing the alloy with porous hosts to make it practical. In 2016, Goodenough and co-workers first proposed using carbon paper to absorb Na-K al-

* Corresponding authors.
E-mail addresses: iamsli@njtech.edu.cn (S. Li), iamfwhuo@njtech.edu.cn (F. Huo).
[1] These authors contributed equally to this work.

https://doi.org/10.1016/j.cclet.2022.107767
1001-8417/© 2023 Published by Elsevier B.V. on behalf of Chinese Chemical Society and Institute of Materia Medica, Chinese Academy of Medical Sciences.

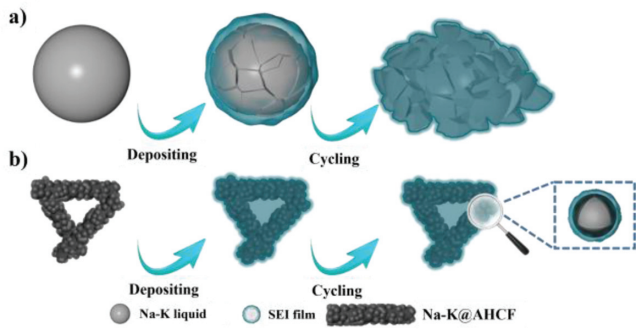

Scheme 1. Schematic diagram of the metal liquid electrodes during the deposition/stripping process. (a) Na-K alloy; (b) Na-K alloy immersed into AHCF host.

loy as an anode for battery systems with a high operating temperature of 420 °C [47]. In 2018, metal foams (Cu, Al and Ni) were introduced as Na-K alloy hosts by vacuum infiltration at RT [48]. In 2019, Zhang *et al.* reported a highly graphitized carbon paper as a host for Na-K alloy by forming a graphite intercalation composite [49]. Although significant progress has been achieved, strategies for constructing composite with liquid metal at RT for practical applications are still highly needed.

Herein, in this work, we have designed an amorphous hollow carbon film (AHCF) as a flexible host for liquid Na-K alloy anode. Specifically, two components are selected for constructing the AHCF: hollow carbon spheres (HCS) and carbon fibers from electrospinning (Scheme S1 in Supporting information). Specifically, HCS was prepared by the hard-template method with SiO_2 and phenol-formaldehyde resin (PF) [50,51]. The as-prepared HCS was then added and dispersed in the polyacrylonitrile (PAN) and DMF solution as precursors for electrospinning. After collecting and annealing the obtained film in the N_2 atmosphere, the AHCF can be obtained.

When immersing the AHCF into the Na-K alloy, the liquid metal can be rapidly adsorbed and infiltrated into the hollow host, forming a Na-K@AHCF electrode. More experimental details can be found in the supporting materials. The designed AHCF host is expected to play a significant role in the following aspects. First, as the spheres are hollow and amorphous with abundant defects, the AHCF possesses a rapid adsorption ability to Na-K alloy. Namely, the liquid alloy can be infiltrated inside the hollow carbon spheres according to the surface defects adsorption and capillarity phenomena, forming the Na-K@AHCF electrode. In addition, Scheme 1 shows the schematic diagram of pure Na-K alloy and Na-K@AHCF during the deposition/stripping cycling processes. The hollow structure could offer sufficient space for Na-K liquid alloy volume change during charge/discharge processes. The separated hollow carbon spheres can also isolate the liquid metal droplets, providing better tolerance for electrode failure from volume changing. Further, the carbon-based matrix can improve its coulombic efficiency by providing skeletons to stabilize SEI, avoiding the continuous formation of interfaces between LMA and electrolytes. As a result, the Na-K@AHCF electrode could improve electrochemical performance compared to the K metal. When matching with cathode material of sulfurized polyacrylonitrile (SPAN), the obtained K-S battery could exhibit good cycle stability and rate performance. The design would provide a strategy for promoting the development of liquid metal anode.

To identify the morphologies of the synthesized HCS, AHCF and Na-K@AHCF, scanning electron microscopy (SEM) and transmission electron microscopy (TEM) with an energy dispersive spectrometer (EDS) were used. From Fig. 1, it can be found that most HCS and precursors have spherical morphologies, uniform size (the diam-

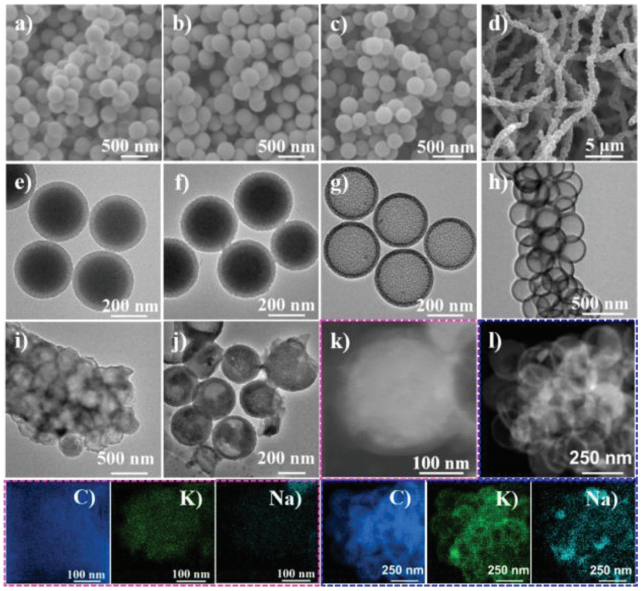

Fig. 1. SEM and TEM images of (a, e) SiO_2@PF/SiO_2, (b, f) SiO_2@C/SiO_2, (c, g) HCS and (d, h) AHCF. (i, j) TEM images of Na-K@AHCF. (k, l) STEM images of Na-K@AHCF and corresponding elemental mapping images of C, K and Na.

eter is about 350 nm) and similar wall thickness (about 20 nm). It should be noted that from Fig. 1g, the walls of HCS are full of open pores, which could offer paths for the liquid alloy to be infiltrated into the cavity. Besides, from Figs. 1d and h, after electrospinning and carbonization, the AHCF presented a uniform distribution of hollow spheres in and on the fiber, presenting an open and hollow grapes-like structure. With the contribution of HCS, there exist plenty of pores and defects of AHCF on the surface. Apart from these, morphologies and internal structures of the carbonized PAN fibers were also characterized by SEM and TEM (Fig. S1 in Supporting information).

After adsorbing Na-K alloy at RT, it can be verified that liquid Na-K alloy has been successfully absorbed on and into the cavities of AHCF and HCS, which could be observed from the TEM images in Figs. 1i and j. To further prove that Na-K alloy can be absorbed into the cavity, the scanning transmission electron microscopy (STEM) at different magnifications (Figs. 1k and l) and their corresponding elemental mapping was presented for the Na-K@AHCF. In Fig. 1k, the carbon wall and Na-K alloy can be distinguished with different contrasts in the STEM image. Combined with the uniform distribution of elemental C, K and Na, it can also be inferred that Na-K alloy is distributed evenly in the cavities.

XRD was applied to identify the composition and crystal structures of the prepared carbon hosts, as shown in Fig. 2a. The AHCF exhibits a similar pattern to the carbonized HCS and carbonized PAN film, which are all amorphous carbon. It suggests that there are plenty of defects on the surface of AHCF cavities, which could lead to the adsorption and infiltration abilities to the liquid alloy. Nitrogen adsorption-desorption isotherms (Fig. 2b) and corresponding pore size distributions (Fig. 2c) are carried out for the hollow materials. The adsorption-desorption curve of HCS shows a typical type IV curve, and the specific surface area can reach 1038.29 cm^3/g. It can be seen from the pore size distribution curve that HCS has a large number of mesopores with diameters of 2–10 nm and microporous. However, the specific surface area of AHCF is only about half that of HCS, 511.88 cm^3/g, and it has a large number of microporous. This is mainly because the precursor HCS accounts for only a component for building AHCF. The carbonized PAN fibers could offer the film better mechanical strength, and the pores and the surface defects of the samples are conducive

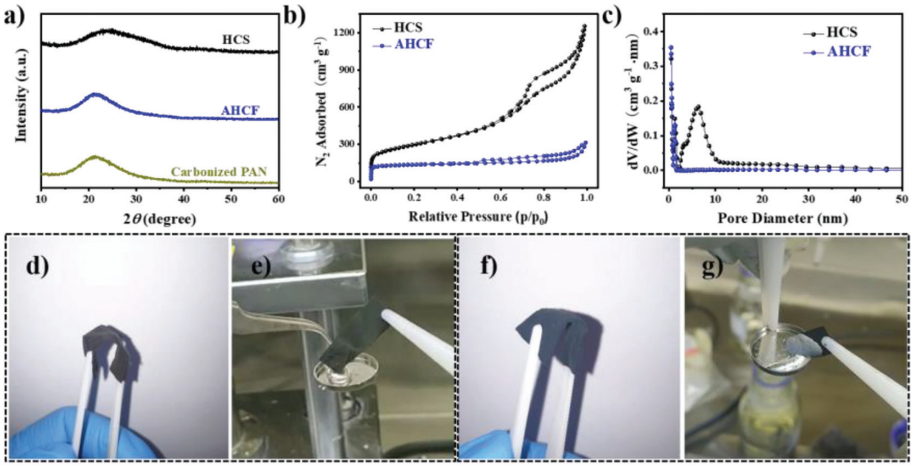

Fig. 2. (a) XRD patterns of HCS, AHCF and carbonized PAN. (b) Nitrogen adsorption-desorption isotherm and (c) the corresponding pore size distribution of HCS and AHCF. Photographs of bent (d) carbonized PAN and (f) AHCF. Photographs of (e) PAN, (g) AHCF contacting with Na-K alloy.

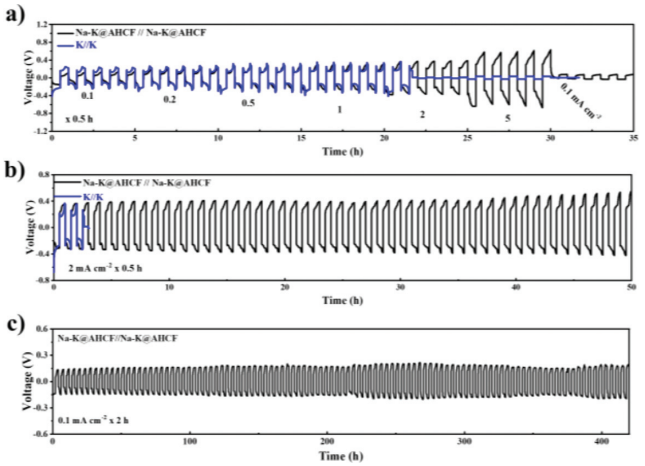

Fig. 3. Electrochemical performance of symmetrical cells cycled in 2 mol/L KFSI EC/DEC electrolytes. (a) Rate performance of Na-K@AHCF//Na-K@AHCF and K//K cells. (b, c) Cycling performance of the cells at different current densities.

to liquid infiltration and adsorption. It also should be noted that the addition of HCS does not significantly reduce the flexibility of AHCF compared with carbonized PAN film. Both the two samples are free-standing and bendable, as shown in Figs. 2d and f.

The carbonized PAN film and AHCF are then emersed into the liquid Na-K alloy to explore the adsorption ability of sample cavities to Na-K alloy. The corresponding photos are shown in Figs. 2e and g, respectively. When contacting with the high-surface-tension liquid alloy, the carbonized PAN cannot be wetted, while AHCF is infiltrated quickly, forming Na-K@AHCF (Videos S2 and S3 in Supporting information). This phenomenon is attributed to the amorphous HCS component, its rich defects and large cavities.

The symmetric cells were assembled with a K-based electrolyte to investigate the electrochemical performance of the Na-K@AHCF. Fig. 3a shows the rate performance of Na-K@AHCF//Na-K@AHCF and K//K metal cells, stripping and depositing at various current densities (0.1, 0.2, 0.5, 1, 2 and 5 mA/cm^2). The Na-K@AHCF cell presents a more stable voltage curve and a lower overpotential compared with the K metal one. The symmetrical cell of K failed after 22 cycles, which may be caused by the unstable interfaces of K metal. In contrast, the Na-K@AHCF exhibited enhanced cycling stability and rate performance. At a high current density of 2 mA/cm^2, a similar phenomenon also can be observed in Fig. 3b, in which Na-K@AHCF//Na-K@AHCF exhibits enhanced cycle stability than the K//K electrodes.

Moreover, the contributions of the hollow structure can also be reflected by the cycle life up to over 400 h at the current density of 0.1 mA/cm^2 (Fig. 3c), showing good cycling stability. However, it should be noted that the polarization values become smaller at about 200 h and 350 h. It is probably due to the liquid volume

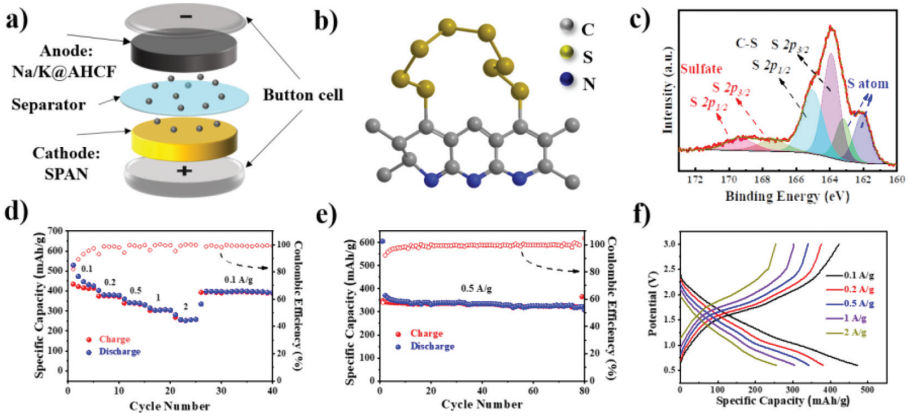

Fig. 4. Electrochemical performance of full cells of K-S battery with SPAN and Na-K@AHCF. The structure schematic of (a) the K-S batteries and (b) SPAN. (c) High-resolution XPS spectrum of S 2p in SPAN. (d) Rate performance and (e) cycle stability of the K-S battery. (f) Galvanostatic charging/discharging curves at various current densities.

changes in the hollow cavities, and some liquid will seep outside the carbon. Therefore, the electrode conductivity would change during cycling, causing variations in the polarization potentials.

In order to characterize the full cell performance, a cathode material of SPAN with a high capacity and long cycle stability was prepared [52–54]. Fig. 4a shows a schematic diagram of a K-S battery using Na-K@AHCF anode and SPAN cathode. The corresponding schematic structure of SPAN is also shown in Fig. 4b. The survey scan and corresponding high-resolution spectrum of C 1s and S 2p are shown in Fig. S4 (Supporting information) and Fig. 4c, proving the successful preparation of the SPAN. The rate performance and cycle stability of this K-S battery are studied in a KFSI in EC/DEC electrolyte with a cycling voltage window from 0.5 V to 3 V (Figs. 4d and e). Under the current density of 0.1, 0.2, 0.5, 1 and 2 A/g, the discharge capacity of the cell can reach 400.4, 380.2, 341.3, 304.4 and 252.4 mAh/g, respectively. At a current density of 0.5 A/g, the capacity did not decrease significantly after 80 cycles. The galvanostatic charge/discharge curves at various current densities are also shown in Fig. 4f, according to a typical K-SPAN battery. Thus, it can be confirmed that when matched with cathode materials of SPAN, Na-K@AHCF anode exhibits excellent electrochemical performance, showing practical application prospects.

In summary, we designed and presented a flexible and free-standing film with a hollow carbon structure, which could enable fast adsorption of Na-K liquid alloy as a host. The designed Na-K@AHCF composite can tolerate the volume expansion of the metal anode during charge/discharge processes and form a more stable interface. As a result, both symmetrical cells of Na-K@AHCF and full K-S battery can exhibit excellent rate performance and cycle stability. The concept of the host design could offer inspiration for advanced alkali metal batteries.

Declaration of competing interest

The authors declare that they have no known competing financial interests or personal relationships that could have appeared to influence the work reported in this paper.

Acknowledgment

This work was financially supported by the National Natural Science Foundation of China (No. 51702155).

Supplementary materials

Supplementary material associated with this article can be found, in the online version, at doi:10.1016/j.cclet.2022.107767.

References

[1] F. Xu, Y. Zhai, E. Zhang, et al., Angew. Chem. Int. Ed. 59 (2020) 19460–19467.
[2] M. Shao, C. Sun, T. Chen, et al., J. Energy Chem. 65 (2022) 127–132.
[3] J. Xiang, L. Yang, L. Yuan, et al., Joule 3 (2019) 2334–2363.
[4] H. Wang, D. Yu, C. Kuang, et al., Chem 5 (2019) 313–338.
[5] B.Y. Ma, P. Bai, Adv. Energy Mater. 12 (2022) 2102967.
[6] G. Liang, X. Li, Y. Wang, et al., Nano Res. Energy 1 (2022) 9120002.
[7] X. Cao, X. Ren, L. Zou, et al., Nat. Energy 4 (2019) 796–805.
[8] Y. Zhao, K.R. Adair, X. Sun, Energy Environ. Sci. 11 (2018) 2673–2695.
[9] S. Liu, J. Mao, Q. Zhang, et al., Angew. Chem. Int. Ed. 59 (2019) 3638–3644.
[10] X. Liang, Q. Pang, I.R. Kochetkov, et al., Nat. Energy 2 (2017) 17119.
[11] C. Qin, D. Wang, Y. Liu, et al., Nat. Commun. 12 (2021) 7184.
[12] X. Li, J. Liu, C. Chen, et al., Chin. Chem. Lett. 32 (2021) 983–989.
[13] R. Chen, A.M. Nolan, J. Lu, et al., Joule 4 (2020) 812–821.
[14] F. Jiang, S. Yang, X. Cheng, et al., J. Energy Chem. 72 (2022) 158–165.
[15] P. Jaumaux, J. Wu, D. Shanmukaraj, et al., Adv. Funct. Mater. 31 (2021) 2008644.
[16] H. Sun, G. Zhu, X. Xu, et al., Nat. Commun. 10 (2019) 3302.
[17] S. Choudhury, S. Wei, Y. Ozhabes, et al., Nat. Commun. 8 (2017) 898.
[18] N. Xiao, W.D. McCulloch, Y. Wu, J. Am. Chem. Soc. 139 (2017) 9475–9478.
[19] Y. Zhao, L.V. Goncharova, A. Lushington, et al., Adv. Mater. 29 (2017) 1606663.
[20] Y. Zhao, L.V. Goncharova, Q. Zhang, et al., Nano Lett. 17 (2017) 5653–5659.
[21] I.D. Seymour, A. Aguadero, J. Mater. Chem. A 9 (2021) 19901–19913.
[22] N. Wu, P.H. Chien, Y. Qian, et al., Angew. Chem. Int. Ed. 59 (2019) 4131–4137.
[23] T. Famprikis, P. Canepa, J.A. Dawson, et al., Nat. Mater. 18 (2019) 1278–1291.
[24] Y. Shen, Y. Zhang, S. Han, et al., Joule 2 (2018) 1674–1689.
[25] X. Guo, J. Bae, Y. Ding, et al., Adv. Funct. Mater. 31 (2021) 2010863.
[26] D. Lin, Y. Liu, Z. Liang, et al., Nat. Nanotechnol. 11 (2016) 626–632.
[27] G. Zheng, S.W. Lee, Z. Liang, et al., Nat. Nanotechnol. 9 (2014) 618–623.
[28] S. Liu, S. Tang, X. Zhang, et al., Nano Lett. 17 (2017) 5862–5868.
[29] L. Ye, M. Liao, T. Zhao, et al., Angew. Chem. Int. Ed. 58 (2019) 17054–17060.
[30] B. Sun, P. Li, J. Zhang, et al., Adv. Mater. 30 (2018) 1801334.
[31] X. Guo, L. Zhang, Y. Ding, et al., Energy Environ. Sci. 12 (2019) 2605–2619.
[32] K. Wang, K. Jiang, B. Chung, et al., Nature 514 (2014) 348–350.
[33] Z. Li, J.T. Zhang, Y.M. Chen, et al., Nat. Commun. 6 (2015) 8850.
[34] G. Liu, J.Y. Kim, M. Wang, et al., Adv. Energy Mater. 8 (2018) 1703652.
[35] X. Lu, G. Li, J.Y. Kim, et al., Nat. Commun. 5 (2014) 4578.
[36] X. Guo, Y. Ding, G. Yu, Adv. Mater. 33 (2021) 2002577.
[37] X. Guo, Y. Ding, H. Gao, et al., Adv. Mater. 32 (2020) 2000316.
[38] Y. Ding, X. Guo, Y. Qian, et al., Adv. Mater. 32 (2020) 2002577.
[39] S. Wei, S. Xu, A. Agrawral, et al., Nat. Commun. 7 (2016) 11722.
[40] D. Guo, J. Qin, Z. Yin, et al., Nano Energy 45 (2018) 136–147.
[41] X. Guo, Y. Ding, L. Xue, et al., Adv. Funct. Mater. 28 (2018) 1804649.
[42] A.C. Baclig, G. McConohy, A. Poletayev, et al., Joule 2 (2018) 1287–1296.
[43] M. Huang, B. Xi, Z. Feng, et al., Small 15 (2019) 1804916.
[44] L. Qin, W. Yang, W. Lv, et al., Chem. Commun. 54 (2018) 8032–8035.
[45] L. Zhang, Y. Li, S. Zhang, et al., Small Methods 3 (2019) 1900383.
[46] C. Liu, H.Y. Chen, W.T. Deng, et al., J. Phys. Chem. Lett. 12 (2021) 9321–9327.
[47] L. Xue, H. Gao, W. Zhou, et al., Adv. Mater. 28 (2016) 9608–9612.
[48] L. Xue, W. Zhou, S. Xin, et al., Angew. Chem. Int. Ed. 57 (2018) 14184–14187.
[49] L. Zhang, S. Peng, Y. Ding, et al., Energy Environ. Sci. 12 (2019) 1989–1998.
[50] H. Zhang, O. Noonan, X. Huang, et al., ACS Nano 10 (2016) 4579–4586.
[51] J. Ding, H. Zhang, H. Zhou, et al., Adv. Mater. 31 (2019) 1900429.
[52] T.H. Hwang, D.S. Jung, J.S. Kim, et al., Nano Lett. 13 (2013) 4532–4538.
[53] Z. Li, J. Zhang, Y. Lu, et al., Sci. Adv. 4 (2018) eaat1687.
[54] S. Li, H. Dai, Y. Li, et al., Energy Storage Mater. 18 (2019) 222–228.